Ab Initio Rate Constants for Unimolecular Reactions: Eliminations of HX from CH_3CH_2X and DX from CD_3CD_2X (X = Cl, Br)

M. P. McGrath* and F. S. Rowland

Department of Chemistry, University of California, Irvine, California 92697

Received: April 18, 2002; In Final Form: June 18, 2002

Usefully accurate rate constant data are calculated ab initio for the four titled unimolecular reactions. The issue of what levels of electronic structure theory are necessary to obtain near quantitative agreement with the observed rate constants is explored. In particular, wave function-based energy barriers, extrapolated to the approximate complete basis set limit, are needed. DFT-based methods significantly underestimate the barrier heights. Considering the various sources of theoretical error, the classical 1,2 HX elimination barriers are 62.7 ± 0.4 kcal/mol for chloroethane and 60.7 ± 0.6 kcal/mol for bromoethane. 1,1 HX elimination is a barrierless process yielding products higher in energy than the CX bond dissociation products.

Introduction

Advances in electronic structure theory have made possible the calculation of simple reaction energies, involving small ideal gas-phase molecules, to useful accuracy (ca. ±1 kcal/mol on average).[1] Although such thermochemical computations are currently only practical for molecules including up to about six non-hydrogen atoms, that includes many systems of great interest in atmospheric chemistry. However, on a given potential energy surface, in contrast to the situation described above for well to well reaction energies, the calculation of well to transition structure (dividing surface) energies is more difficult because ±1 kcal/mol uncertainty in a reaction barrier height does not necessarily lead to usefully accurate rate data, especially at lower temperatures.

For the well-studied 1,2 elimination of HCl from chloroethane, which is a textbook[2,3] example of a prominent barrier unimolecular reaction

$$CH_3CH_2Cl \rightarrow HCl + CH_2CH_2 \qquad (1)$$

a ±1 kcal/mol uncertainty in the barrier height contributes an uncertainty to the rate constant ratio k_{true}/k_{calc} of $e^{\pm 503.2/T}$ (e.g., a factor of 2 at $T = 726$ K). As part of our continuing study of elimination reactions of relevance in atmospheric chemistry,[4,5] reaction 1 and the not as well-studied reaction 2

$$CH_3CH_2Br \rightarrow HBr + CH_2CH_2 \qquad (2)$$

were chosen as test cases to calibrate the accuracy possible for calculating the rate constants of such reactions ab initio, using highly correlated levels of electronic structure theory. As will be shown, the dynamics of both elementary reactions are particularly simple, leaving the calculation of the barrier heights of reactions 1 and 2 (including the fully deuterated isotopomers) as a major factor in determining the accuracy of the rate constants subsequently derived. With our best results, near quantitative agreement with the accepted experimental rate data is obtained for CH_3CH_2Cl and CD_3CD_2Cl. Although the lack of definitive experimental rate data for the bromine systems over an extended temperature range complicates our analysis, at least at one applicable temperature our best results again show near quantitative agreement with the observed rate data.

Although the results mentioned above were achieved using wave function-based methods of electronic structure theory, we also consider the performance of commonly used variations of density functional theory for computing the barrier heights of reactions 1 and 2. Compared to our best, albeit more computationally intensive molecular orbital theory results, density functional theory variants underestimate the classical 1,2 elimination barrier heights by 3−12 kcal/mol.

Finally, we also obtain reaction profiles for the 1,1 HX elimination reactions

$$CH_3CH_2Cl \rightarrow HCl + CH_3CH \qquad (3)$$

$$CH_3CH_2Br \rightarrow HBr + CH_3CH \qquad (4)$$

on their respective potential energy surfaces. Taking account of our calculated $\Delta H_f(0)$ of the carbene CH_3CH, it is easily seen why elementary reactions 3 and 4 have not been observed.

Theoretical Methods

Stationary point structures on the singlet C_2H_5X (X = Cl, Br) potential energy surfaces were optimized at the restricted Hartree−Fock (RHF) and quadratic configuration interaction (QCISD)[6] levels of electronic structure theory[7,8] using the cc-pVDZ basis set.[9] Force constant matrixes and related normal mode harmonic vibrational frequencies (see below for the isotopes used) were calculated for each stationary point, either analytically (RHF) or using central differences of analytical energy gradients (QCISD). Full intrinsic reaction coordinate (IRC)[10] calculations were made for each stationary point corresponding to a transition structure (TS), thus connecting each TS with a pair of minima (reactant and product). The IRCs were obtained using a nuclear stepsize of 0.1 $amu^{1/2}$ Bohr and atomic masses corresponding to $^{12}C_2{}^1H_5X$ or $^{12}C_2D_5X$, where X = ^{35}Cl, ^{79}Br and D = ^2H. Subsequent QCISD geometry optimization and force constant matrix determinations were also made using the diffuse spd function augmented, aug-cc-pVDZ basis set.[9,11]

10.1021/jp020986u CCC: $22.00
Published on Web 08/09/2002

Single point energies were calculated at the QCISD(T)[6] and CCSD(T)[12] levels of theory using the cc-pVNZ (N = D, T, Q) basis sets[9] on the QCISD/cc-pVDZ optimized geometries. For convenience, we use the shortened lowercase acronym "vnz" to refer to the actual cc-pVNZ basis set and "avdz" to refer to the aug-cc-pVDZ basis set. As with the QCISD optimization/force constant determinations, only the valence electrons of C ($2s^22p^2$), Cl ($3s^23p^5$), and Br ($4s^24p^5$) were explicitly included in the post RHF electron correlation treatments. Approximate correlation energy extrapolations[13] to the vnz basis limit (v∞z), E_∞^{corr}, were made using five different formulas suggested in the literature[14−16]

$$E^{corr}(l) = E_\infty^{corr} + Al^{-3} \quad (5)$$

$$E^{corr}(l) = E_\infty^{corr} + A(l + 0.5)^{-4} \quad (6)$$

$$E^{corr}(l) = E_\infty^{corr} + Al^{-3} + Al^{-4}(-0.9766 + 6.1793e^{1.0940A}) \quad (7)$$

$$E^{corr}(l) = E_\infty^{corr} + A(l + 0.5)^{-B} \quad (8)$$

$$E^{corr}(l) = E_\infty^{corr} + A(l + 0.5)^{-4} + B(l + 0.5)^{-6} \quad (9)$$

where $l = 2$ for vdz, $l = 3$ for vtz, $l = 4$ for vqz, and E_∞^{corr}, A, and B are fitted parameters. In the two parameter eqs 5−7, exact fits were made using $E^{corr}(3)$ and $E^{corr}(4)$, whereas in the three parameter eqs 8−9, exact fits were made using $E^{corr}(2)$, $E^{corr}(3)$, and $E^{corr}(4)$. For reactions 1 and 2, the ΔE_∞^{corr} were combined with ΔE_∞^{RHF} to yield approximate QCISD(T)/v∞z and CCSD(T)/v∞z classical barrier heights ΔE. It was not necessary to use extrapolations to obtain ΔE_∞^{RHF}, as tests showed convergence to ±0.01 kcal/mol is already obtained at v5z. As each formula gave slightly different results, the average of the five ΔE_∞^{corr} was used.

To gauge the effect of core electron correlation on the ΔE, QCISD(T) energies in which all electrons were explicitly correlated were calculated using the G3large basis set.[1] This basis set, approximately of vtz quality, also contains tight, high exponent α Gaussian basis functions optimized for correlating inner shell electrons: $\alpha_p = 16$, $\alpha_d = 15$ for C; $\alpha_d = 13$, $\alpha_f = 12$ for Cl; and $\alpha_d = 68$, $\alpha_f = 7$ for Br. In addition, multireference configuration interaction (MR-CISD) calculations[17] were used to test the applicability of the single-reference QCISD(T) and CCSD(T) methods on the TSs, which were found to have certain very elongated bond distances.

Energy and energy derivative computations on the C_2H_5Cl and C_2H_5Br potential energy surfaces were made with the *Gaussian 98*[18] and *Molpro*[19] program suites. To assess the accuracy of density functional theory (DFT) methods for the HX elimination barrier heights of reactions 1 and 2, a variety of electron density functionals built into *Gaussian 98* were tried. Both normal (pure DFT) and hybrid (i.e., using some RHF exchange) functionals were tried, 25 of the former (all combinations of 5 exchange and 5 correlation functionals) and 5 of the latter.[20] Included among the various functionals is the B-LYP functional often used in Car-Parrinello type simulations, as well as its related and often used three parameter hybrid functional B3-LYP.[21] The DFT optimization/force constant determinations that were carried out are analogous to those described above for RHF/vdz, except that for B-LYP and B3-LYP, the vtz basis set was used as well.

Results and Discussion

1,1 Elimination. As discussed in the Introduction, the endothermic unimolecular production of HX can in principle occur by 1,2 (reactions 1 and 2) or 1,1 elimination (reactions 3 and 4), respectively producing either ethenes or isomeric carbenes. RHF and QCISD potential energy surface scans (constrained geometry optimizations) using both vdz and avdz basis sets agree that 1,1 elimination proceeds without barrier to give the HX + CH_3CH products, which in fact are even higher in energy than the homolytic X + CH_3CH_2 channel. This is shown on the relative enthalpy (0 K) scale of Figure 1, where the $\Delta H_f(0)$ of CH_3CH (89.2 kcal/mol), derived from its G3[1] atomization energy (457 kcal/mol), was used. Since the 1,2 elimination TSs (vide infra) are lower in energy than X + CH_3-CH_2, the important thermal HX elimination pathways are via reactions 1 and 2, and indeed reaction 3 could not be observed.[22]

1,2 Elimination. From the point of view of the reverse of reaction 1, the electrophilic addition of HCl to ethene, there have been three relatively recent mechanistic studies using correlated levels of electronic structure theory.[23−25] Although the end goal of these studies is not the same as ours (calculation of rate constants), for valuable mechanistic insight refs 23−25 should be consulted. In the following sections, we make comparisons wherever possible to analogous experimental data. Although we believe our comparisons to previous work are apt, they are also necessarily incomplete, and we leave for a review comparisons to other relevant experimental and theoretical data.

Physical Properties. The theoretical HX elimination TSs for reactions 1 and 2 are defined in Tables 1 and 2. Their symmetry and shape are in general agreement with the study of Toto et al.,[26] who reported RHF level TSs for all of the haloethanes and compared them to previous (semiempirical) models conjectured for the 1,2 elimination TSs.

Both RHF/vdz and QCISD/vdz IRCs (Figures 1S and 2S) are qualitatively similar, showing profiles for reactions 1 and 2 commencing from the staggered CH_3CH_2X reactant conformations, through the eclipsed conformations (identified by the shoulder on the reactant side of each IRC), over the pronounced barriers, and then on to the CH_2CH_2 + HX products. The latter form intermolecular C_2H_4·HX complexes of C_{2v} point group symmetry that have been observed using microwave spectroscopy.[27,28] After forming the eclipsed conformation by internal rotation, each reaction maintains a symmetry plane along the rest of the IRC. The four stationary points encountered along each IRC are shown in Figure 2, including key QCISD/avdz geometrical parameters from Tables 1 and 2. Comparison of the theoretical (r_e) geometrical parameters of the staggered reactants and intermolecular product complexes with those determined from microwave spectroscopy (r_s)[27−30] demonstrates satisfactory agreement between the different sets of parameters, the main differences being the somewhat longer (by 0.02−0.03 Å) theoretical CX bond lengths of the reactants. As might be expected, the diffuse spd functions in the avdz basis set lead to improved intermolecular distances in the QCISD structures of C_2H_4·HX.

The magnitudes of the theoretical electric dipole moments (μ_e) of CH_3CH_2X (Tables 1 and 2) are also in satisfactory agreement with the experimental (μ_0) determinations.[31] Although the staggered to eclipsed internal rotation barely changes the (roughly 2 D) dipole moments, at the HX elimination TSs the very elongated CX bonds result in QCISD dipole moments in the 5−6 D range. That the TSs are necessarily very polar was deduced in 1963 by Benson and Bose in their analysis of the available rate data.[32] It might be supposed that such very polar TSs would show significant multireference character in their electronic structures, yet test MR-CISD calculations using various active space references consistently resulted in wave

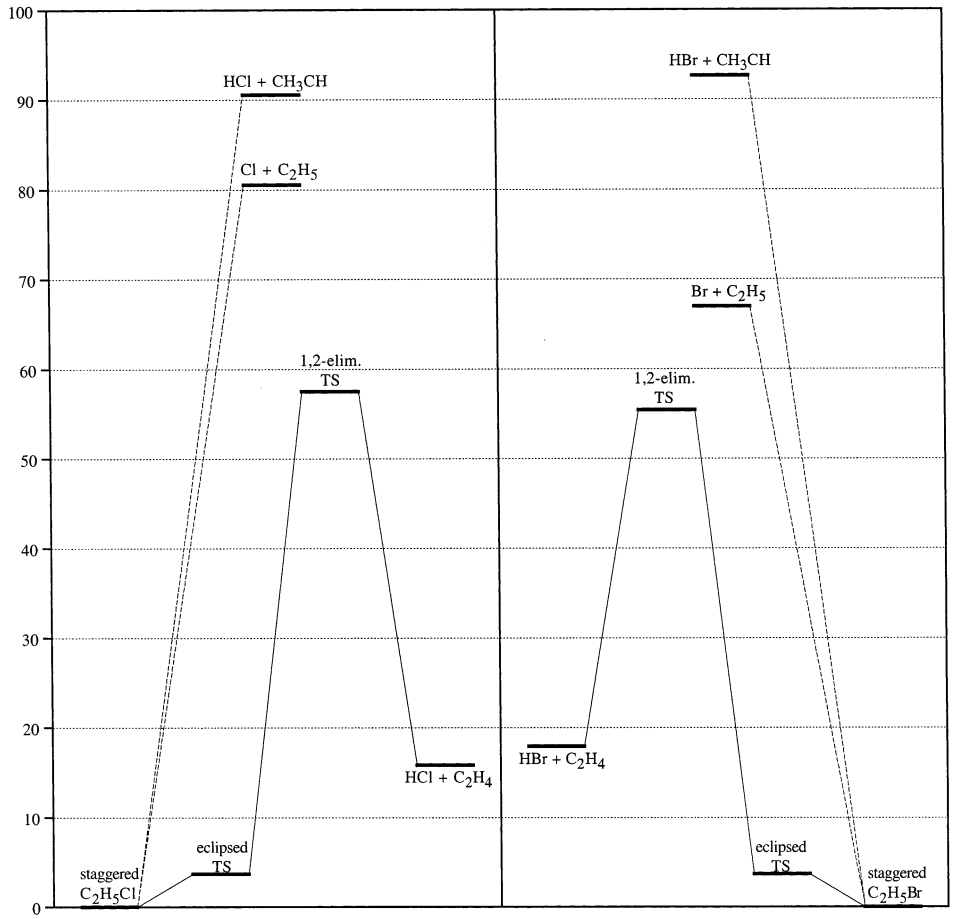

Figure 1. Relative enthalpy (0 K) scale for stationary points on the C_2H_5Cl and C_2H_5Br potential energy surfaces (kcal/mol). Empirical[54] $\Delta H_f(0)$ are used, except for CH_3CH and the elimination TSs (see text).

TABLE 1: C_2H_5Cl Optimum Equilibrium and Saddle Point Structures, Dipole Moments, and Energies[a]

method	r(H′C$_2$)	r(C$_2$C$_1$)	r(C$_1$Cl)	r(H′Cl)	r(C$_2$H)	r(C$_1$H)	∠(H′C$_2$C$_1$)	∠(C$_2$C$_1$Cl)	∠(C$_1$C$_2$H)	∠(C$_2$C$_1$H)	τ(HC$_2$C$_1$H′)	τ(HC$_1$C$_2$C$_l$)	$\lvert\mu\rvert$	$-538 - E$
staggered H′CH$_2$CH$_2$Cl (C_s)[b]														
RHF/ vdz	1.093	1.514	1.807	3.713	1.090	1.087	109.2	111.4	111.0	112.1	±119.6	±118.5	2.39	0.15902
QCISD/ vdz	1.106	1.524	1.807	3.732	1.104	1.102	109.6	111.2	110.8	111.7	±119.8	±118.9	2.01	0.63048
/avdz	1.105	1.525	1.818	3.737	1.102	1.099	109.4	110.9	110.8	112.1	±119.7	±118.3	2.17	0.65985
observed[e]	*[1.092]*	*1.520*	*1.789*	*3.70*	*[1.092]*	*1.089*	*109.3*	*111.0*	*110.4*	*111.6*	*±120.2*	*±118.7*	*2.05*	
eclipsed H′CH$_2$CH$_2$Cl TS (C_s)[b]														
RHF/ vdz	1.088	1.531	1.809	2.705	1.091	1.086	111.4	112.6	110.8	112.3	±120.1	±118.6	2.38	0.15238
QCISD/ vdz	1.102	1.541	1.809	2.708	1.104	1.101	111.1	112.5	110.9	112.0	±120.0	±119.1	2.01	0.62412
/avdz	1.100	1.542	1.821	2.707	1.103	1.099	111.1	112.2	110.8	112.3	±120.0	±118.4	2.16	0.65412
H′Cl elim. H′CH$_2$CH$_2$Cl TS (C_s)[b]														
RHF/ vdz	1.241	1.383	2.701	1.934	1.082	1.080	75.3	93.3	119.2	121.6	±100.9	±87.9	8.07	0.05495
QCISD/ vdz	1.273	1.411	2.564	1.780	1.096	1.095	80.8	90.0	118.3	121.7	±104.1	±90.3	5.21	0.52349
/avdz	1.262	1.410	2.600	1.839	1.094	1.093	78.3	91.8	118.8	121.5	±102.2	±89.5	5.86	0.56143
C_2H_4·H′Cl (C_{2v})[b,c]														
RHF/ vdz		1.323	(4.033)[d]	1.281	1.084				121.6		±90.3		1.94	0.13268
QCISD/ vdz		1.349	(3.858)	1.292	1.097				121.5		±90.2		1.88	0.60217
/avdz		1.351	(3.727)	1.296	1.095				121.5		±90.2		1.80	0.63223
observed[f]			*(3.724)*											

[a] Units: interatomic lengths r in angstroms, interatomic angles ∠ and dihedral angles τ in degrees, electric dipole moments μ in debyes, and total electronic energies E in hartrees. [b] H′, C$_2$, C$_1$, and Cl are in the symmetry plane. [c] Cl, H′, and the C═C bond midpoint are on the 2-fold symmetry axis. [d] Distance between Cl and the C═C bond midpoint. [e] Microwave structure (r_s) from ref 29 (parameters in brackets assumed equal); dipole moment (μ_0) from ref 31. [f] Microwave structure from ref 27.

functions dominated by the RHF configurations. For example, selecting the 18 most important configurations from 20 electrons in 14 orbitals complete active space references resulted in MR-CISD/vdz wave functions for the TSs with RHF configuration coefficients of 0.92. In such circumstances, the size-consistent single reference QCISD(T) and CCSD(T) methods should, by virtue of their perturbational correlation energy contributions for triple electron excitations from the RHF references, give usefully accurate 1,2 elimination barrier heights, as long as the basis set requirements are met.

In Table 3, theoretical values of the reduced moments of inertia I_r and 3-fold energy barriers V_3 for the internal rotations of the reactants are given, as well as the analogous experimentally determined values.[33−37] There is significant improvement

TABLE 2: C_2H_5Br Optimum Equilibrium and Saddle Point Structures, Dipole Moments, and Energies[a]

method	r(H′C$_2$)	r(C$_2$C$_1$)	r(C$_1$Br)	r(H′Br)	r(C$_2$H)	r(C$_1$H)	∠(H′C$_2$C$_1$)	∠(C$_2$C$_1$Br)	∠(C$_1$C$_2$H)	∠(C$_2$C$_1$H)	τ(HC$_2$C$_1$H′)	τ(HC$_1$C$_2$Br)	$\lvert\mu\rvert$	$-2650 - E$
staggered H′CH$_2$CH$_2$Br (C_s)[b]														
RHF/ vdz	1.094	1.515	1.966	3.864	1.090	1.086	109.0	111.7	111.2	112.4	±119.5	±118.0	2.39	1.04093
QCISD/ vdz	1.106	1.525	1.968	3.884	1.103	1.101	109.3	111.4	111.0	112.2	±119.7	±118.4	1.98	1.49107
/avdz	1.105	1.526	1.974	3.884	1.102	1.099	109.3	111.1	110.9	112.3	±119.6	±117.9	2.15	1.51883
observed[e]	*[1.092]*	*1.519*	*1.950*	*3.84*	*[1.092]*	*1.087*	*108.8*	*111.1*	*110.6*	*112.3*	*±120.1*	*±117.8*	*2.03*	
eclipsed H′CH$_2$CH$_2$Br TS (C_s)[b]														
RHF/ vdz	1.088	1.532	1.968	2.828	1.091	1.085	112.0	113.1	110.5	112.7	±120.3	±118.2	2.38	1.03428
QCISD/ vdz	1.102	1.541	1.971	2.830	1.104	1.100	111.8	112.9	110.7	112.4	±120.2	±118.6	1.98	1.48472
/avdz	1.100	1.542	1.976	2.828	1.103	1.098	111.7	112.7	110.6	112.6	±120.1	±118.1	2.14	1.51303
H′Br elim. H′CH$_2$CH$_2$Br TS (C_s)[b]														
RHF/ vdz	1.242	1.381	2.894	2.110	1.082	1.081	74.5	94.3	119.4	121.5	±99.9	±87.4	8.77	0.94241
QCISD/ vdz	1.250	1.416	2.836	1.943	1.097	1.097	87.4	85.4	117.6	121.5	±106.4	±88.1	5.38	1.38899
/avdz	1.254	1.412	2.825	1.978	1.095	1.094	82.2	88.9	118.5	121.4	±103.4	±88.2	6.01	1.42283
C_2H_4·H′Br (C_{2v})[b,c]														
RHF/ vdz		1.323	(4.292)[d]	1.415	1.084				121.6		±90.3		1.62	1.01283
QCISD/ vdz		1.348	(4.083)	1.427	1.097				121.5		±90.2		1.58	1.46050
/avdz		1.351	(3.929)	1.432	1.095				121.5		±90.2		1.51	1.48690
observed[f]			*(3.916)*											

[a] Units: interatomic lengths r in angstroms, interatomic angles ∠ and dihedral angles τ in degrees, electric dipole moments μ in debyes, and total electronic energies E in hartrees. [b] H′, C$_2$, C$_1$, and Br are in the symmetry plane. [c] Br, H′, and the C=C bond midpoint are on the 2-fold symmetry axis. [d] Distance between Br and the C=C bond midpoint. [e] Microwave structure (r_s) from ref 30 (parameters in brackets assumed equal); dipole moment (μ_0) from ref 31. [f] Microwave structure from ref 28.

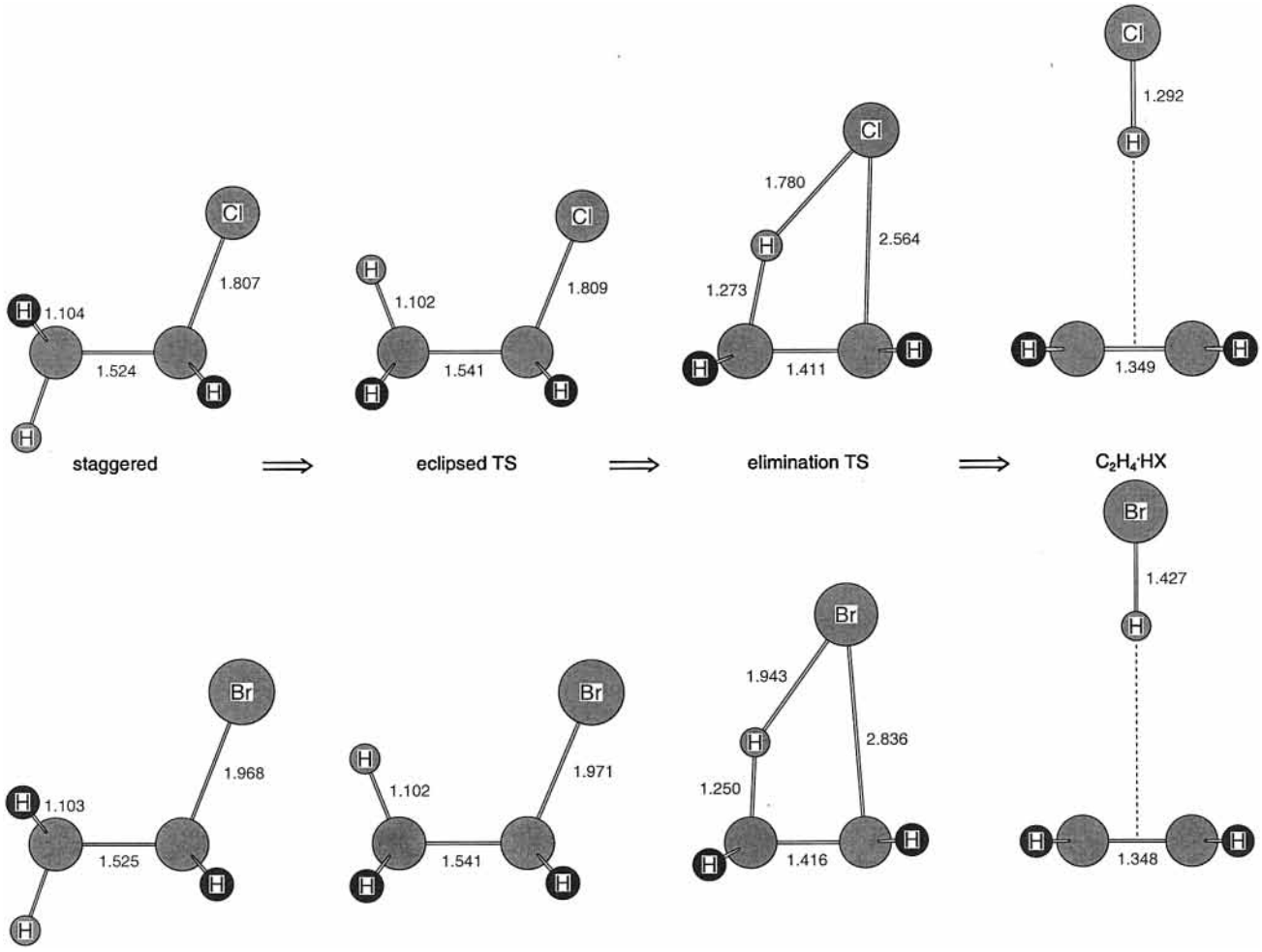

Figure 2. Stationary point structures encountered along the IRCs for 1,2 HX elimination from CH_3CH_2Cl and CH_3CH_2Br. Selected QCISD/avdz geometrical parameters (Å) are labeled. The plane of the figure is a mirror plane of symmetry, so two hydrogen atoms are hidden.

in the classical QCISD barriers as the basis set is enlarged from vdz to avdz, the QCISD/avdz V_3 only slightly lower than the experimental ranges shown. The theoretical I_r, which will be used in the rate calculations, reflect the generally satisfactory agreement with the experimental structural parameters shown in Tables 1 and 2. Because the difference in the theoretical I_r of CH_3CH_2X or CD_3CD_2X between the staggered (Table 3) and eclipsed forms is only about 1%, using a constant value of I_r to describe each internal rotation is acceptable.

Also required for the rate calculations are sets of normal mode vibrational frequencies for C_2H_5X and C_2D_5X at the elimination TS and reactant geometries. Sets of such harmonic vibrational

TABLE 3: Reduced Moments of Inertia (amu Å^2) and Barriers to Internal Rotation (cm^{-1}) for CH_3CH_2X, X = Cl, Br[a]

method	I_r	V_3
	CH_3CH_2Cl	
RHF/ vdz	3.067	1457
QCISD/ vdz	3.140	1394
/avdz	3.137	1257
observed	*3.155*,[b] *3.161*[c,d]	*1260*,[b] *1289*,[c] *1290*[d]
	CH_3CH_2Br	
RHF/ vdz	3.123	1461
QCISD/ vdz	3.200	1393
/avdz	3.194	1271
observed	*3.151*,[e] *3.182*[f]	*1282*,[e] *1288*[f]

[a] To obtain the I_r for CD_3CD_2X, multiply by 1.941 (X = Cl) or 1.975 (X = Br). [b] Ref 33. [c] Ref 34. [d] Ref 35. [e] Ref 36. [f] Ref 37.

frequencies (ω_e) corresponding to the same three theoretical methods as in Tables 1−3 are listed in Tables 4 and 5, along with the spectroscopically determined fundamentals (ω_0) of the reactants.[38−40] The average absolute deviation (AAD) between the theoretical and observed haloethane frequencies decreases with improved theoretical methodology. For the total of 72 modes of CH_3CH_2X and CD_3CD_2X (X = Cl, Br), the AAD decreases from 8.7% at RHF/vdz, to 3.3% at QCISD/vdz, to 2.4% at QCISD/avdz. In particular, the torsional mode ω_{18} is the most sensitive to the theoretical method used, as might be expected from the comparisons of Table 3. It was necessary to estimate the ω_{15} fundamentals of CH_3CH_2Br and CD_3CD_2Br (whose calculated infrared intensities are indeed very weak), based on the differences between the QCISD/avdz and observed frequencies for the analogous modes of CH_3CH_2Cl and CD_3CD_2Cl. Our estimates for ω_{15} are 1245 cm^{-1} for CH_3CH_2Br and 976 cm^{-1} for CD_3CD_2Br, which in each reported spectrum are near the strong ω_7 bands centered at 1244 and 986 cm^{-1}, respectively.

In the rate calculations, rigid rotor-harmonic oscillator partition functions will be employed.[41] The theoretical harmonic vibrational frequency sets are therefore directly applicable, although theoretical ω_e are in general too large compared to the limited number of polyatomic molecules for which empirically derived ω_e are available. Although using a different uniform scaling factor (in the 0.89−0.99 range)[42] for each of the three theoretical methods in Tables 4 and 5 might be expected to help alleviate this trend, we have decided on an ab initio approach and have not scaled the theoretical ω_e for two reasons. First, it is not clear that the ω_e of TSs are necessarily amenable to the same (method dependent) scaling factors suggested for minima. Second, after realizing that the lowest frequencies make the biggest contributions to the vibrational partition functions, it is clear from the lower frequency QCISD data in Tables 4 and 5 that scaling by a uniform factor less

TABLE 4: Observed Fundamental and Calculated Harmonic Vibrational Frequencies (cm^{-1}) of C_2H_5Cl and C_2D_5Cl[a]

mode			RHF/vdz	QCISD/vdz	QCISD/avdz			
sym.	no.	*observed*	% deviation	% deviation	% deviation	RHF/vdz	QCISD/vdz	QCISD/avdz
			CH_3CH_2Cl				HCl elim. TS	
A′	1	*2985.1*	9.4	5.6	4.6	3357	3203	3194
	2	*[2954]*	10.1	5.3	4.9	3302	3166	3155
	3	*2943.9*	8.2	4.1	3.4	1813	1600	1615
	4	*1467.0*	9.0	2.2	1.6	1647	1471	1485
	5	*1458.9*	9.4	2.4	1.7	1563	1432	1449
	6	*1383.9*	10.0	2.5	1.8	1424	1300	1308
	7	*1288.5*	10.2	3.1	2.2	1193	1046	1078
	8	*1072.7*	8.8	2.8	2.3	1120	968	989
	9	*973.1*	7.9	3.2	2.1	338	334	329
	10	*677.0*	3.9	2.6	−0.2	272	303	274
	11	*334.4*	6.2	0.6	0.0	1147*i*	1795*i*	1504*i*
A″	12	*3011.5*	10.4	5.6	5.1	3474	3313	3305
	13	*2987.6*	9.8	5.7	5.0	3409	3269	3258
	14	*1447.3*	9.3	2.6	2.0	1348	1258	1249
	15	*1251.0*	9.3	2.3	1.6	1324	1225	1221
	16	*[1082]*	6.9	0.2	−0.3	887	826	823
	17	*785.1*	7.3	0.6	−0.1	878	747	775
	18	*250.5*	13.6	9.6	3.8	330	369	359
			CD_3CD_2Cl				DCl elim. TS	
A′	1	*2226*	8.6	4.9	3.8	2459	2343	2335
	2	*2172*	9.1	4.2	3.8	2396	2293	2286
	3	*2128*	7.7	3.6	2.8	1539	1412	1416
	4	*1165*	10.1	3.8	2.8	1263	1086	1096
	5	*1079*	8.3	1.6	0.8	1160	1061	1078
	6	*1056*	8.5	1.8	1.1	1068	989	995
	7	*1022*	8.9	2.5	1.3	938	812	839
	8	*893*	8.4	2.6	2.1	829	716	732
	9	*780*	7.4	2.1	1.0	309	319	309
	10	*622*	4.8	2.6	0.2	256	274	251
	11	*297*	6.4	0.7	0.0	851*i*	1335*i*	1118*i*
A″	12	*2266*	9.1	4.2	3.8	2593	2470	2464
	13	*2248*	8.3	4.3	3.5	2545	2438	2430
	14	*1052*	8.3	1.6	1.0	1072	996	994
	15	*976*	8.6	1.5	0.9	962	894	887
	16	*800*	8.3	1.9	1.4	631	591	589
	17	*577*	7.1	0.3	−0.3	627	532	552
	18	*184.2*	12.7	8.7	2.9	237	265	258
	avg. abs. dev. (36)		8.6	3.2	2.1			

[a] Spectroscopic frequencies from ref 38 (those in brackets are from an empirical force field analysis).

TABLE 5: Observed Fundamental and Calculated Harmonic Vibrational Frequencies (cm^{-1}) of C_2H_5Br and C_2D_5Br[a]

mode			RHF/vdz	QCISD/vdz	QCISD/avdz			
sym.	no.	*observed*	% deviation	% deviation	% deviation	RHF/vdz	QCISD/vdz	QCISD/avdz
			CH_3CH_2Br				HBr elim. TS	
A′	1	*2975*	9.9	5.8	4.9	3354	3192	3185
	2	*2963*	9.9	5.3	4.8	3305	3153	3148
	3	*2927*	8.7	4.6	3.9	1820	1597	1601
	4	*1456*	9.5	2.9	2.3	1639	1465	1470
	5	*1447*	10.0	2.9	2.2	1563	1430	1417
	6	*1380*	10.1	2.6	2.0	1427	1282	1288
	7	*1244*	11.2	3.8	3.5	1189	1047	1055
	8	*1065*	8.7	2.9	2.4	1142	986	1011
	9	*960*	8.5	3.3	2.6	292	290	251
	10	*562*	5.9	3.9	2.8	221	203	220
	11	*294*	4.4	−1.0	−1.4	1031*i*	1663*i*	1477*i*
A″	12	*3020*	10.5	5.6	5.1	3472	3301	3296
	13	*2985*	10.0	5.9	5.1	3414	3252	3250
	14	*1445*	9.5	2.8	2.3	1332	1269	1249
	15	*[1245]*	9.2	2.0	1.6	1323	1218	1214
	16	*1023*	9.1	1.9	1.9	893	821	819
	17	*780*	6.0	−0.8	−1.3	881	656	717
	18	*249*	13.3	9.2	4.0	301	312	323
			CD_3CD_2Br				DBr elim. TS	
A′	1	*2240*	7.8	4.0	3.0	2458	2333	2328
	2	*2183*	8.8	3.9	3.5	2397	2284	2280
	3	*2117*	8.2	4.0	3.3	1547	1402	1409
	4	*1159*	10.1	3.7	2.8	1252	1082	1086
	5	*1070*	8.7	1.9	1.2	1160	1042	1034
	6	*1052*	8.8	2.0	1.4	1069	984	990
	7	*986*	10.4	3.8	3.1	935	779	819
	8	*897*	7.4	1.8	1.4	847	766	751
	9	*748*	8.8	2.4	2.0	264	270	237
	10	*520*	5.2	2.9	1.9	207	185	198
	11	*261*	5.0	−0.8	−1.1	762*i*	1238*i*	1097*i*
A″	12	*2269*	9.4	4.4	4.0	2591	2461	2458
	13	*2224*	9.6	5.5	4.6	2549	2424	2423
	14	*1051*	8.4	1.7	1.1	1071	993	992
	15	*[976]*	8.4	1.3	0.9	951	900	883
	16	*763*	8.0	1.0	1.2	636	590	587
	17	*570*	6.7	0.0	−0.5	629	465	509
	18	*180*	13.9	9.4	4.4	215	223	231
	avg. abs. dev. (36)		8.8	3.4	2.7			

[a] Spectroscopic frequencies from ref 39, 40 (those in brackets are semiempirical estimates; see text).

than unity will not always be helpful. For example, the QCISD ω_{11} of CH_3CH_2Br and CD_3CD_2Br are already lower than the observed (anharmonic) fundamentals.

As a minor refinement in the rate calculations, the lowest frequency of each staggered reactant, ω_{18} of A″ symmetry, is omitted from the vibrational partition function and replaced by an internal rotation partition function q_{ir}. That is, the data of Tables 3−5 are used in the q_{ir} defined by Ayala and Schlegel.[43] There is no analogous torsional mode for the HX elimination TSs because of the very elongated CX and incipient HX bonds (Figure 2). These structural changes result in the lowest A″ frequency for each of the elimination TSs being higher than three other modes of A′ symmetry, and depending on the system and theoretical method, 40−100 cm^{-1} higher than ω_{18} of the reactant. Therefore, all of the real normal modes of the elimination TSs are treated as vibrations in the rate constant calculations.

Energy Barriers. Because of the expected strong dependence of the calculated rate data on the values of the classical barrier heights for HX elimination, ΔE, we sought to obtain QCISD(T) and CCSD(T) values of ΔE for reactions 1 and 2 corresponding to the complete basis set limit. As discussed, eqs 5−9 were used to extrapolate the correlation energies of the reactants and the HX elimination TSs to their vnz limits. For each reaction, the arithmetic mean and standard deviation from the mean of each set of five ΔE obtained are shown in Table 6, along with the barrier heights at vdz, vtz, and vqz. In each case, increasing basis set flexibility decreases ΔE. The RHF limit barrier heights obtained for reactions 1 and 2 are 67.5 and 63.8 kcal/mol, respectively. Therefore, post RHF electron correlation effects lower ΔE by 3.1−5.2 kcal/mol, depending on the reaction and correlation method. Because the approximate v∞z ΔE are 0.4−0.5 kcal/mol larger at CCSD(T) than at QCISD-

TABLE 6: Energy Barriers for HCl and HBr Elimination (kcal/mol)

method \ basis set	vdz	vtz	vqz	v∞z[a]
	$CH_3CH_2Cl \rightarrow HCl + CH_2CH_2$			
DFT[b]	51.1−53.4			
hybrid DFT[c]	56.8−59.5			
RHF	65.3			
QCISD(T)[d]	65.6	63.8	62.8	62.3 ± 0.2
CCSD(T)[d]	66.0	64.3	63.2	62.7 ± 0.2
	$CH_3CH_2Br \rightarrow HBr + CH_2CH_2$			
DFT[b]	48.4−51.6			
hybrid DFT[c]	54.5−57.3			
RHF	61.8			
QCISD(T)[d]	62.7	61.8	60.8	60.2 ± 0.3
CCSD(T)[d]	63.3	62.4	61.5	60.7 ± 0.3

[a] See text for details of the extrapolations to the approximate basis set limit. [b] Results from 25 different functionals. [c] Results from 5 different hybrid functionals. [d] QCISD/vdz geometries (Tables 1 and 2) used.

TABLE 7: Dependencies of the Energy Barriers for HCl and HBr Elimination (kcal/mol) on Geometry and Core Correlation Effects

method \ geometry	QCISD/vdz	QCISD/avdz
	$CH_3CH_2Cl \rightarrow HCl + CH_2CH_2$	
CCSD(T)/vtz	64.25	64.43
QCISD(T)/vtz	63.83	64.01
QCISD(T) = full − QCISD(T)	(0.20)[a]	
	$CH_3CH_2Br \rightarrow HBr + CH_2CH_2$	
CCSD(T)/vtz	62.42	62.38
QCISD(T)/vtz	61.77	61.80
QCISD(T) = full − QCISD(T)	(0.33)[a]	

[a] Core correlation $\Delta\Delta E$ values obtained with the G3large (ref 1) basis set.

(T), both classical barriers will be used in parallel in the rate constant calculations for reactions 1 and 2.

The approximate v∞z values of ΔE at QCISD(T) and CCSD(T) given in Table 6 correspond to energy differences between QCISD/vdz stationary point structures. To get a feeling for the geometry dependence of the ΔE, we show in Table 7 how the barrier heights change when the stationary point structures are refined from QCISD/vdz to QCISD/avdz (Tables 1 and 2). Using the vtz basis, for both QCISD(T) and CCSD(T), the ΔE increase by about 0.2 kcal/mol for C_2H_5Cl but hardly change for C_2H_5Br. Because these changes are minor, we assume the QCISD/vdz structures are adequate representations of the unknown exact (r_e) geometries of the HX elimination TSs and CH_3CH_2X.

The adequacy of the frozen core approximation used in the barrier height computations was also tested. By explicitly correlating all electrons (at much increased computational time) and using a basis set optimized for core correlation effects, one can see how each barrier height so calculated varies from that calculated using the same basis set within the frozen core approximation. The results of such computations at the QCISD(T)/G3large level are also shown in Table 7, where it is seen that core correlation effects increase ΔE by 0.2 kcal/mol for C_2H_5Cl and by 0.3 kcal/mol for C_2H_5Br.

In summary, variations in the barrier height energies for reactions 1 and 2 from: using different correlation energy extrapolation formulas (±0.2 to ±0.3 kcal/mol), using different stationary point geometries (0−0.2 kcal/mol), and removing the frozen core approximation (0.2−0.3 kcal/mol) leads to likely uncertainties for the ΔE of ±0.4 kcal/mol for CH_3CH_2Cl and ±0.6 kcal/mol for CH_3CH_2Br. The effect of differential scalar relativistic effects on the ΔE are not likely to be as important as the three effects discussed, because the geometries of each isomeric pair (reactant and elimination TS) are closely related. Also, primary basis set superposition errors in the ΔE are minimized because they tend to vanish in the complete basis limit. The computed single point energies for the reactants and elimination TSs are listed in Table 1S.

Returning to Table 6, the respective QCISD(T) and CCSD(T) ΔE for CH_3CH_2Cl, 62.3 and 62.7 kcal/mol, can be compared to the DFT and hybrid DFT ΔE, where for each electron density functional optimization/force constant computations were carried out using the vdz basis set. Analogous computations using the larger vtz basis set with the B-LYP and B3-LYP functionals resulted in negligible differences (<0.1 kcal/mol) of ΔE from the vdz values. It can be concluded from the data of Table 6 that DFT underestimates the barrier height of reaction 1 by roughly 10 kcal/mol. Hybrid DFT performs better, but still underestimates ΔE significantly. For reaction 2, the conclusions are similar. Compared to the respective QCISD(T) and CCSD(T) ΔE for CH_3CH_2Br, 60.2 and 60.7 kcal/mol, DFT again underestimates the barrier by around 10 kcal/mol, whereas the hybrid DFT underestimation is not as severe. Again, the basis set dependence of the DFT-based results is slight, as vtz computations with B-LYP and B3-LYP decrease the vdz ΔE by less than 0.2 kcal/mol. It should be noted that the highest DFT-based ΔE were obtained using the hybrid MPW1-PW91 functional.[20] In contrast to DFT, RHF overestimates the barrier heights and as expected shows a stronger basis set dependence. Analogous RHF/vtz computations decrease the RHF/vdz ΔE by 0.4 kcal/mol for C_2H_5Cl and by 1.2 kcal/mol for C_2H_5Br.

Rate Constants. The RRKM theory of unimolecular reactions reduces to transition state theory in the high-pressure limit.[2,3] Given that experimental rate constants for reactions 1 and 2 are available in this (pressure independent) regime, we calculated transition state theory rate constants $k(T)$ for the HX eliminations of CH_3CH_2X and the DX eliminations of CD_3CD_2X (X = Cl, Br), and used the experimental rate data to gauge the accuracy of the ab initio $k(T)$. For these reactions, variational and canonical transition state theory are equivalent for our purposes, as the maximum point in each IRC (at reaction coordinate $s = 0$) also corresponds to the point of maximum free energy, within the 0.1 amu$^{1/2}$ Bohr gridsize for s used to obtain each IRC. That is, in the ca. 500−1000 K temperature range relevant to reactions 1 and 2, $G(T)$ is higher at $s = 0$ than at $s = \pm 0.1$ amu$^{1/2}$ Bohr for each of the four processes. Therefore, the theoretical dynamics reduce to the simple rate constant expression

$$k(T) = \Gamma \frac{k_B T}{h} \frac{Q_{TS}}{Q_{EtX}} e^{-\Delta E/k_B T} \tag{10}$$

where the $Q = q_{tra}\, q_{rot}\, q_{ir}\, q_{vib}$ are total partition functions[41] of the staggered reactants and elimination TSs, Γ is a tunneling correction factor, k_B is Boltzmann's constant, and h is Planck's constant.

Besides the first-order Wigner tunneling factor,[44] which makes use of the calculated imaginary vibrational frequencies $\omega^{\ddagger}$ of the elimination TSs (ω_{11} in Tables 4 and 5) and speed of light c

$$\Gamma_{Wigner}(T) = 1 + \frac{1}{24} \left| \frac{hc\omega^{\ddagger}}{k_B T} \right|^2 \tag{11}$$

we also calculated the semiclassical (WKB) tunneling correction[44] for each IRC $V(s)$

$$\Gamma_{WKB}(T) = 1 + \frac{2}{k_B T} \int_{V_0}^{V_{max}} \sinh\left(\frac{V_{max} - E}{k_B T}\right) [1 + e^{2R(E)}]^{-1}\, dE \tag{12}$$

In eq 12, $V_0 = \max[V(s_{reactant}), V(s_{product})]$, $V_{max} = V(0)$, and

$$R(E) = \frac{4\pi\sqrt{2}}{h} \int_{s_<}^{s_>} \sqrt{V(s) - E}\, ds \tag{13}$$

In eq 13, $s_<$ is the negative value of s where $V(s_<) = E$ on the reactant side of each IRC, and $s_>$ is the positive value of s where $V(s_>) = E$ on the product side of each IRC. The integration in eqs 12 and 13 was straightforwardly carried out by increasingly subdividing each integral (5 point Gauss-Legendre quadrature for each subintegral) until convergence was obtained. The factor $[1 + e^{2R(E)}]^{-1}$ in eq 12 is actually the barrier transmission (tunneling) probability at energies $V_0 \le E \le V_{max}$ and is exactly 0.5 at $E = V_{max}$, increasing to unity for $E > 2V_{max} - V_0$.[44] Instead of the semiclassical transmission probability, the exact probability can easily be used, provided the $V(s)$ are first fit to

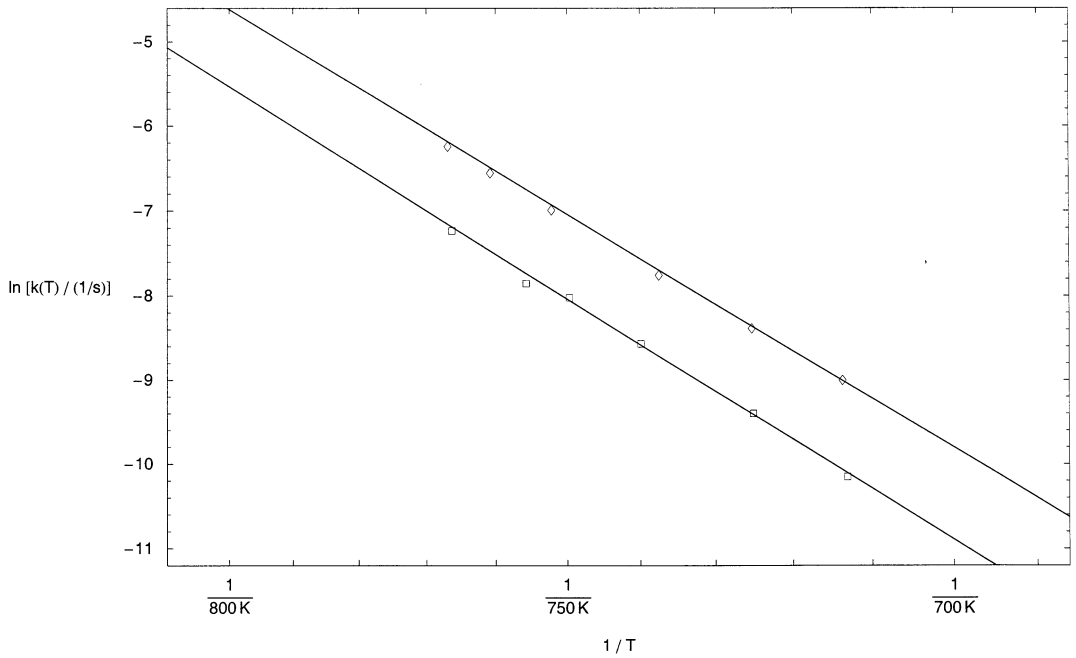

Figure 3. Arrhenius plots of the best (see text) ab initio unimolecular rate constants for CH_3CH_2Cl (upper curve) and CD_3CD_2Cl (lower curve), alongside the experimental rate data of Heydtmann and co-workers.[48,49]

a convenient functional form.[45] But if care is taken to fit the IRCs especially well near the top of the barrier, the two approaches were found to yield similar $\Gamma(T)$. Note that because the $V(s)$ are mass dependent, having wider shaped barriers (for a given X) for C_2D_5X than for C_2H_5X, the $\Gamma(T)$ are uniformly lower for the heavier DX elimination reaction. Using QCISD/vdz data, Γ_{WKB} (Γ_{Wigner}) for C_2H_5Cl, C_2D_5Cl, C_2H_5Br, and C_2D_5Br at 700 K are, respectively, 1.84 (1.57), 1.49 (1.31), 1.67 (1.49), and 1.46 (1.27). These relatively small tunneling correction factors suggest (but do not prove) the appropriateness of using one-dimensional $\Gamma(T)$.

Experimental gas-phase kinetics of the thermal decomposition (pyrolysis) of the haloethanes has an extensive literature. For example, in their 1992 study Huybrechts et al.[46] give nine references for reaction 1 alone. The literature up to 1970 has been included in the review by Benson and O'Neal.[47] At least for CH_3CH_2Cl and CD_3CD_2Cl, accepted[2] values of the unimolecular elimination $k(T)$ in the high-pressure limit are available. Heydtmann and co-workers[48,49] have reported first-order rate data for CH_3CH_2Cl and CD_3CD_2Cl between 713 and 767 K at pressures ranging from 0.1 to 300 Torr. They find that at 100 Torr, the reactions are already in the pressure independent regime, and their rate constants at 725.2 K are shown in Table 8. Kairaitis and Stimson[50] have made a careful study of the thermal decomposition of CH_3CH_2Br at 423.1° (696.25 K) and their high pressure (143−322 Torr) rate constant for reaction 2 is also shown in Table 8. For CD_3CD_2Br, we make use of the high-pressure H/D kinetic isotope effect (KIE) expression reported by Blades et al.[51] to deduce k(696.25 K) for CD_3CD_2Br. Note that the Blades et al. KIE expression was obtained for k_H/k_D relative rates at 731−965 K and we are assuming that our extrapolation to 696.25 K does not contribute to the uncertainty in the rate constant.

Comparing the observed and ab initio rate constants shown in Table 8, it is evident that the best theoretical results are obtained using the approximate CCSD(T)/v∞z barriers, along with QCISD/vdz data and Γ_{WKB}. Assuming no uncertainty in the four experimental rate constants, this theoretical procedure gives an AAD from experiment of 3.5% (using Γ_{Wigner} increases the AAD to 9.5%, whereas using no correction gives an AAD of 35%). Indeed, the necessity of including a tunneling correction has been discussed previously for the reverse of reaction 1.[24]

TABLE 8: Dependence of Theoretical Unimolecular Rate Constants $k(T)/(10^{-4}\ s^{-1})$ on Computational Details and Comparisons with Experiment

		QCISD(T) barrier[a]		CCSD(T) barrier[b]	
haloethane	tunneling function	RHF data[c]	QCISD data[d]	RHF data[c]	QCISD data[d]
CH_3CH_2Cl		*k(725.2 K) = 2.27±0.05*[e]			
	WKB	1.90	3.08	1.44	2.33
	Wigner	1.80	2.68	1.36	2.03
	none	1.48	1.75	1.12	1.33
CD_3CD_2Cl		*k(725.2 K) = 0.83±0.02*[f]			
	WKB	0.78	1.09	0.59	0.82
	Wigner	0.74	0.97	0.56	0.73
	none	0.66	0.75	0.50	0.57
CH_3CH_2Br		*k(696.25 K) = 2.53±0.08*[g]			
	WKB	1.48	3.96	1.03	2.76
	Wigner	1.40	3.52	0.98	2.45
	none	1.18	2.36	0.82	1.64
CD_3CD_2Br		*k(696.25 K) = 0.97±0.17*[g,h]			
	WKB	0.59	1.40	0.41	0.98
	Wigner	0.57	1.22	0.39	0.85
	none	0.51	0.96	0.36	0.67

[a] Using approximate QCISD(T)/v∞z barrier (Table 6). [b] Using approximate CCSD(T)/v∞z barrier (Table 6). [c] Using RHF/vdz moments of inertia, vibrational frequencies, internal rotation barriers, and IRCs. [d] Using QCISD/vdz moments of inertia, vibrational frequencies, internal rotation barriers, and IRCs. [e] Observed rate constant from ref 48. [f] Observed rate constant from ref 49. [g] Observed rate constant from ref 50. [h] Rate constant obtained using the H/D KIE expression of ref 51.

Because the rate constants in Table 8 are only at a single temperature for each reaction, it is of interest to show the theoretical (as defined above) Arrhenius plots alongside all the high-pressure data of Heydtmann and co-workers.[48,49] As shown in Figure 3, for CH_3CH_2Cl and CD_3CD_2Cl there is near quantitative agreement between experiment and theory at all six temperatures for each reaction. Assuming no uncertainty in the experimental rate constants, the AAD between the theoretical

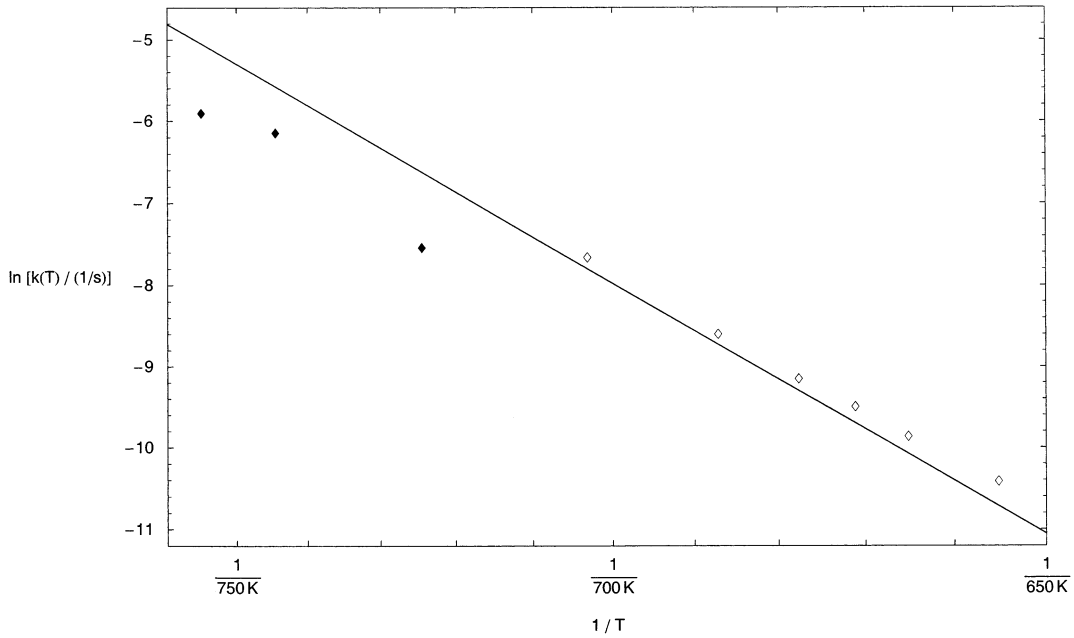

Figure 4. Arrhenius plots of the best (see text) ab initio unimolecular rate constants for CH_3CH_2Br, alongside the experimental rate data of Thomas[52] (open symbols) and Park and Jung[53] (filled symbols).

and experimental rate constants corresponding to the twelve points in Figure 3 is 4.8%.

As has long been recognized experimentally, for CH_3CH_2Br the interference of simultaneous radical chain reactions must be taken into account before the unimolecular (reaction 2) rate can be ascertained.[32,50,52] For this and other reasons (e.g., surface effects), unimolecular rate data for CH_3CH_2Br over a significant temperature range, of precision comparable to that obtained by Heydtmann and co-workers for chloroethane, have not been reported. Nevertheless, in Figure 4 we show the theoretical Arrhenius plot for CH_3CH_2Br alongside the experimental rate data of Thomas,[52] whose early kinetic study is the one preferred by Benson and O'Neal[47] for bromoethane. Note that the $k(696.25\ K) = 3.1 \times 10^{-4}\ s^{-1}$ interpolated from Thomas' rate data is not too different from the presumably accurate value ($2.53 \times 10^{-4}\ s^{-1}$)[50] shown in Table 8. Also shown in Figure 4 are the high-pressure unimolecular rate constants for reaction 2 reported in 1980 by Park and Jung at three higher temperatures.[53] As is apparent in Figure 4, the theoretical curve lies inbetween the two, seemingly incompatible, experimental data sets. New measurements of the high pressure rate constants of reaction 2, especially in the temperature range of Figure 4, would certainly be of interest. Additionally, although we have used the Blades et al.[51] H/D KIE expression to infer the experimental k(696.25 K) for CD_3CD_2Br, it is likely that at increasing temperatures (up to 965 K) their expression increasingly underestimates the KIE.

Conclusions

For the 1,2 elimination reactions of CH_3CH_2Cl and CD_3CD_2Cl, rate constants calculated ab initio reproduce the accepted high pressure, 713−767 K experimental rate data with an average absolute deviation of 5%. This near quantitative agreement serves to validate the computational procedures used: approximate CCSD(T)/v∞z classical energy barrier, along with QCISD/vdz physical properties and semiclassical tunneling corrections. Indeed, for the 1,2 elimination reactions of CH_3CH_2Br and CD_3CD_2Br, results of similar quality are obtained at 696 K using the same procedures. Using combinations of other computational procedures—including approximate QCISD(T)/v∞z barriers, RHF/vdz physical properties, and Wigner tunneling corrections—still lead to reasonable (within a factor of 3) rate constants for the four reactions, but that would not be the case using barriers corresponding to any of the 30 electron density functionals tested.

Acknowledgment. The research was supported by an allocation of computer resources through Network and Academic Computing Services at UCI.

Supporting Information Available: IRCs for 1,2 HX elimination from CH_3CH_2X and 1,2 DX elimination from CD_3CD_2X, X = Cl, Br (supplementary Figures 1S and 2S); total electronic energies for CH_3CH_2X and HX elimination TSs, X = Cl, Br (supplementary Table 1S). This material is available free of charge via the Internet at http://pubs.acs.org.

References and Notes

(1) (a) Curtiss, L. A.; Redfern, P. C.; Rassolov, V.; Kedziora, G.; Pople, J. A. *J. Chem. Phys.* **2001**, *114*, 9287. (b) Curtiss, L. A.; Raghavachari, K.; Redfern, P. C.; Rassolov, V.; Pople, J. A. *J. Chem. Phys.* **1998**, *109*, 7764.

(2) Gilbert, R. G.; Smith, S. C. *Theory of Unimolecular and Recombination Reactions*; Blackwell Scientific: Oxford, 1990.

(3) Holbrook, K. A.; Pilling, M. J.; Robertson, S. H. *Unimolecular Reactions*, 2nd ed.; Wiley: New York, 1996.

(4) Dubey, M. K.; McGrath, M. P.; Smith, G. P.; Rowland, F. S. *J. Phys. Chem. A* **1998**, *102*, 3127.

(5) McGrath, M. P.; Rowland, F. S., manuscript in preparation.

(6) Pople, J. A.; Head-Gordon, M.; Raghavachari, K. *J. Chem. Phys.* **1987**, *87*, 5968.

(7) Hehre, W. J.; Radom, L.; Schleyer, P. v. R.; Pople, J. A. *Ab Initio Molecular Orbital Theory*; John Wiley: New York, 1986.

(8) Jensen, F. *Introduction to Computational Chemistry*; John Wiley: New York, 1999.

(9) Wilson, A. K.; Woon, D. E.; Peterson, K. A.; Dunning Jr., T. H. *J. Chem. Phys.* **1999**, *110*, 7667, and references therein.

(10) (a) Gonzalez, C.; Schlegel, H. B. *J. Phys. Chem.* **1990**, *94*, 5523. (b) Baboul, A. G.; Schlegel, H. B. *J. Chem. Phys.* **1997**, *107*, 9413.

(11) Kendall, R. A.; Dunning Jr., T. H.; Harrison, R. J. *J. Chem. Phys.* **1992**, *96*, 6796.

(12) Raghavachari, K.; Trucks, G. W.; Pople, J. A.; Head-Gordon, M. *Chem. Phys. Lett.* **1989**, *157*, 479.

(13) Klopper, W.; Bak, K. L.; Jorgensen, P.; Olsen, J.; Helgaker, T. *J. Phys. B* **1999**, *32*, R103.

(14) (a) Halkier, A.; Helgaker, T.; Jorgensen, P.; Klopper, W.; Koch, H.; Olsen, J.; Wilson, A. K. *Chem. Phys. Lett*. **1998**, *286*, 243. (b) Truhlar, D. G. *Chem. Phys. Lett*. **1998**, *294*, 45.

(15) Martin, J. M. L. In *Computational Thermochemistry*, ACS Symp. Ser. 677; Irikura, K. K. and Frurip, D. J., Eds.; American Chemical Society: Washington D. C., 1998; p 212.

(16) Varandas, A. J. C. *J. Chem. Phys.* **2000**, *113*, 8880.

(17) (a) Werner, H.-J.; Knowles, P. J. *J. Chem. Phys.* **1988**, *89*, 5803. (b) Knowles, P. J.; Werner, H.-J. *Chem. Phys. Lett.* **1988**, *145*, 514.

(18) Frisch, M. J.; Trucks, G. W.; Schlegel, H. B.; Scuseria, G. E.; Robb, M. A.; Cheeseman, J. R.; Zakrzewski, V. G.; Montgomery Jr., J. A.; Stratmann, R. E.; Burant, J. C.; Dapprich, S.; Millam, J. M.; Daniels, A. D.; Kudin, K. N.; Strain, M. C.; Farkas, O.; Tomasi, J.; Barone, V.; Cossi, M.; Cammi, R.; Mennucci, B.; Pomelli, C.; Adamo, C.; Clifford, S.; Ochterski, J.; Petersson, G. A.; Ayala, P. Y.; Cui, Q.; Morokuma, K.; Malick, D. K.; Rabuck, A. D.; Raghavachari, K.; Foresman, J. B.; Cioslowski, J.; Ortiz, J. V.; Baboul, A. G.; Stefanov, B. B.; Liu, G.; Liashenko, A.; Piskorz, P.; Komaromi, I.; Gomperts, R.; Martin, R. L.; Fox, D. J.; Keith, T.; Al-Laham, M. A.; Peng, C. Y.; Nanayakkara, A.; Gonzalez, C.; Challacombe, M.; Gill, P. M. W.; Johnson, B. G.; Chen, W.; Wong, M. W.; Andres, J. L.; Head-Gordon, M.; Replogle, E. S.; Pople, J. A. *Gaussian 98*, Gaussian, Inc.: Pittsburgh, 1998.

(19) Werner, H.-J.; Knowles, P. J., with contributions from Almlof, J.; Amos, R. D.; Deegan, M. J. O.; Elbert, S. T.; Hampel, C.; Lindh, R.; Meyer, W.; Peterson, K.; Pitzer, R.; Stone, A. J.; Taylor, P. R. *Molpro*, version 96.1.

(20) (a) The Gaussian 98 keywords for the 5 exchange functionals are: S, B, PW91, MPW, and G96; the keywords for the 5 correlation functionals are: VWN5, LYP, PL, P86, and PW91. The Gaussian 98 keywords for the 5 hybrid functionals are: B3-LYP, B3-P86, B3-PW91, B1-LYP, and MPW1-PW91. (b) Frisch, A.; Frisch, M. J. *Gaussian 98 User's Reference*, Gaussian, Inc.: Pittsburgh, 1998, and references therein.

(21) (a) Becke, A. D. *Phys. Rev. A* **1988**, *38*, 3098. (b) Becke, A. D. *J. Chem. Phys*. **1993**, *98*, 5648. (c) Lee, C.; Yang, W.; Parr, R. G. *Phys. Rev. B* **1988**, *37*, 785.

(22) (a) Tang, Y.-N.; Rowland, F. S. *J. Am. Chem. Soc.* **1965**, *87*, 3304. (b) Tang, Y.-N.; Rowland, F. S. *J. Am. Chem. Soc.* **1968**, *90*, 570.

(23) Thorsteinsson, T.; Famulari, A.; Raimondi, M. *Int. J. Quantum Chem.* **1999**, *74*, 231.

(24) Borve, K. J.; Jensen, V. R. *J. Chem. Phys.* **1996**, *105*, 6910.

(25) Menendez, M. I.; Suarez, D.; Sordo, J. A.; Sordo, T. L. *J. Comput. Chem.* **1995**, *16*, 659.

(26) Toto, J. L.; Pritchard, G. O.; Kirtman, B. *J. Phys. Chem.* **1994**, *98*, 8359.

(27) Aldrich, P. D.; Legon, A. C.; Flygare, W. H. *J. Chem. Phys.* **1981**, *75*, 2126.

(28) Fowler, P. W.; Legon, A. C.; Thumwood, J. M. A.; Waclawik, E. R. *Coord. Chem. Rev.* **2000**, *197*, 231.

(29) Hayashi, M.; Inagusa, T. *J. Mol. Struct.* **1990**, *220*, 103.

(30) Inagusa, T.; Hayashi, M. *J. Mol. Spectrosc*. **1988**, *129*, 160.

(31) Nelson Jr., R. D.; Lide Jr., D. R.; Maryott, A. A. *Selected Values of Electric Dipole Moments for Molecules in the Gas Phase*, NSRDS−NBS 10; U. S. Department of Commerce: Washington D. C., 1967.

(32) Benson, S. W.; Bose, A. N. *J. Chem. Phys.* **1963**, *39*, 3463.

(33) Stahl, W.; Dreizler, H.; Hayashi, M. *Z. Naturforsch. A* **1983**, *38*, 1010.

(34) Schwendeman, R. H.; Jacobs, G. D. *J. Chem. Phys.* **1962**, *36*, 1245.

(35) Fateley, W. G.; Kiviat, F. E.; Miller, F. A. *Spectrochimica Acta A* **1970**, *26*, 315.

(36) Gripp, J.; Dreizler, H.; Schwarz, R. *Z. Naturforsch. A* **1985**, *40*, 575.

(37) Flanagan, C.; Pierce, L. *J. Chem. Phys.* **1963**, *38*, 2963.

(38) (a) McKean, D. C.; McQuillan, G. P.; Robertson, A. H. J.; Murphy, W. F.; Mastryukov, V. S.; Boggs, J. E. *J. Phys. Chem.* **1995**, *99*, 8994. (b) Miller, F. A.; Kiviat, F. E. *Spectrochimica Acta A* **1969**, *25*, 1363.

(39) (a) Suzuki, S.; Bribes, J. L.; Gaufres, R. *J. Mol. Spectrosc.* **1973**, *47*, 118. (b) Gaufres, R.; Bejaud-Bianchi, M. *Spectrochimica Acta A* **1971**, *27*, 2249.

(40) Durig, J. R.; Player Jr., C. M.; Bragin, J. *J. Chem. Phys.* **1971**, *54*, 460.

(41) McQuarrie, D. A. *Statistical Mechanics;* Harper and Row: New York, 1973.

(42) Scott, A. P.; Radom, L. *J. Phys. Chem.* **1996**, *100*, 16 502.

(43) Ayala, P. Y.; Schlegel, H. B. *J. Chem. Phys.* **1998**, *108*, 2314. See eq 26 therein.

(44) (a) Bell, R. P. *The Tunnel Effect in Chemistry*; Chapman and Hall: New York, 1980. (b) Truhlar, D. G.; Isaacson, A. D.; Garrett, B. C. In *Theory of Chemical Reaction Dynamics*, Vol. IV.; Baer, M., Ed.; CRC Press: Boca Raton, 1985; p 65.

(45) Ahmed, Z. *Phys. Rev. A* **1993**, *47*, 4761.

(46) Huybrechts, G.; Hubin, Y.; van Mele, B. *Int. J. Chem. Kinetics* **1992**, *24*, 671.

(47) Benson, S. W.; O'Neal, H. E. *Kinetic Data on Gas-Phase Unimolecular Reactions*, NSRDS−NBS 21; U. S. Department of Commerce: Washington D. C., 1970.

(48) Heydtmann, H.; Dill, B.; Jonas, R. *Int. J. Chem. Kinetics* **1975**, *7*, 973.

(49) Jonas, R.; Heydtmann, H. *Ber. Bunsen-Ges. Phys. Chem.* **1978**, *82*, 823.

(50) Kairaitis, D. A.; Stimson, V. R. *Aust. J. Chem.* **1971**, *24*, 2031.

(51) Blades, A. T.; Gilderson, P. W.; Wallbridge, M. G. H. *Can. J. Chem.* **1962**, *40*, 1533.

(52) Thomas, P. J. *J. Chem. Soc.* **1959**, 1192.

(53) Park, T. J.; Jung, K. H. *Bull. Korean Chem. Soc.* **1980**, *1*, 30.

(54) Wagman, D. D.; Evans, W. H.; Parker, V. B.; Schumm, R. H.; Halow, I.; Bailey, S. M.; Churney, K. L.; Nuttall, R. L. *J. Phys. Chem. Ref. Data* **1982**, *11*, Supplement 2.